CrystEngComm

PAPER

Cite this: *CrystEngComm*, 2017, **19**, 1495

Close insight into the nature of intermolecular interactions in dihydropyrimidine-2(1*H*)-thione derivatives†

Aamer Saeed,*[a] Ulrich Flörke,[b] Adolfo Fantoni,[c] Asma Khurshid,[a] Hiram Pérez*[d] and Mauricio F. Erben*[e]

Received 22nd December 2016,
Accepted 12th February 2017

DOI: 10.1039/c6ce02619b

rsc.li/crystengcomm

The crystal structures of four 1-(*R*-phenyl)-4,4,6-trimethyl-3,4-dihydropyrimidine-2(1*H*)-thione derivatives [*R* = 2-chloro (**1**), 2,3-di-chloro (**2**), 2,4-di-methyl (**3**), and 4-methoxy (**4**)] were determined and analysis of their molecular conformations was carried out. A comparative study of the intermolecular interactions—including eight closely related structures from CSD—was performed and the degree of isostructurality was quantified. The intermolecular interactions were characterized in terms of the periodic system electron density and the topological analysis highlighted the role of N–H···S═C hydrogen bonds in the stabilization of the different supramolecular architectures. PIXEL lattice energy calculations revealed that the dispersion component was the major contributor, together with the important role of the Coulombic term to the total energy. The interaction energies for molecular pairs involving N–H···S═C hydrogen bonds indicated a dominant contribution to packing stabilization coming from the Coulombic components. Hirshfeld surfaces and fingerprint plots allowed us to visualize different intermolecular contacts and their relative contributions to the total surface for each compound. Analysis of the electrostatic potentials (ESP) correlated well with the computed energies, thus characterizing the strengths of the different interactions.

1 Introduction

Non-covalent interactions play an essential role in supramolecular chemistry, molecular biology, and crystal engineering.[1] It is well-known that strong hydrogen bonds have been preferably used in the design of materials with specific desirable properties.[2] In the absence of strong hydrogen bonds, however, other types of non-covalent interactions can be dominant and therefore responsible for a crystal's stability. Hydrogen bonds do not represent an exclusively electrostatic interaction but rather a complex combination of at least four components such as electrostatic (acid/base), polarization (hard/soft), van der Waals (dispersion/repulsion), and covalent (charge transfer) interactions. The electrostatic nature is clearly dominant in strong hydrogen bonds, particularly, if the donor and acceptor atoms are very electronegative, but the proportion of electrostatic character can vary, even in the case of weaker interactions. In this direction, the study of non-covalent interactions in sulfur-containing compounds is attracting increasing attention in crystal engineering,[3] mainly because of the high polarizability of the electron density at the sulfur atom. Thus, the versatilities of the thioamide [–C(S)NH_2],[4,5] triazolethione,[6,7] and thiosemicarbazone[8] functional groups as key moieties for crystal engineering have recently been recognized.

[a] *Department of Chemistry, Quaid-I-Azam University, Islamabad 45320, Pakistan. E-mail: aamersaeed@yahoo.com; Fax: +92 51 9064 2241; Tel: +54 221 445 4393*
[b] *Department of Chemistry, University of Paderborn, 33098 Paderborn, Germany*
[c] *Departamento de Física, Facultad de Ciencias Exactas, Instituto de Física La Plata, Universidad Nacional de La Plata, 49 y 115, La Plata, Buenos Aires, República Argentina*
[d] *Departamento de Química Inorgánica, Facultad de Química, Universidad de la Habana, Habana 10400, Cuba. E-mail: hperez@quimica.uh.cu; Fax: +53 78783641; Tel: +53 78703922*
[e] *CEQUINOR (UNLP, CONICET-CCT La Plata), Departamento de Química, Facultad de Ciencias Exactas, Universidad Nacional de La Plata, C.C. 962 (1900), La Plata, República Argentina. E-mail: erben@quimica.unlp.edu.ar; Fax: +54 211 425 9485; Tel: +54 211 425 9485*

† Electronic supplementary information (ESI) available: Ring puckering parameters and endocyclic torsion angles for compounds **1–4** are given in Tables S1 and S2, respectively. Topological and geometrical parameters for the main intermolecular interactions of compounds **1–4** are shown in Tables S3–S6, respectively. Interaction energies for molecular pairs involving H···H contacts and electrostatic potentials in **1–4** and related compounds are shown in Tables S7 and S8, respectively. An overlay diagram for independent molecules of compound **1** is shown in Fig. S1. Packing diagrams as well as the intermolecular energies for the respective molecular pairs for compounds **1–4** are given in Fig. S2–S5, respectively. The Hirshfeld surfaces study of compound **1** is shown in Fig. S6. Fig. S7 shows the relative contributions of the intermolecular contacts to the Hirshfeld surface area, and the full 2D fingerprint plots are displayed in Fig. S8. Hirshfeld surface mapped with electrostatic potentials (ESP) and 3D-deformation density maps for compounds **1–4** are shown in Fig. S9–S12, respectively. CCDC 1504146–1504149. For ESI and crystallographic data in CIF or other electronic format see DOI: 10.1039/c6ce02619b

Dihydropyrimidine-2-thiones are heterocyclic compounds with a pyrimidine ring system.[9,10] This class of compounds is usually obtained by variations of the well-known three-component reaction reported long ago by Pietro Biginelli.[11,12] In recent years, a considerable amount of increased interest has been directed at the role and effect of dihydropyrimidine-2-thiones in a variety of biological activities.[13,14]

In this work, the crystal structures of four novel 1-(*R*-phenyl)-4,4,6-trimethyl-3,4-dihydropyrimidine-2(1*H*)-thione derivatives [see Scheme 1, *R* = 2-chloro (**1**), 2,3-dichloro (**2**), 2,4-dimethyl (**3**) and 4-methoxy (**4**)], were determined using single-crystal X-ray analysis.

The aims of the present study were: (1) to analyze the conformational stability of the 3,4-dihydropyrimidine-2(1*H*)-thione moiety by varying the phenyl substitution at the 1-position, and (2) to determine the intermolecular interactions governing the crystal structure of the 3,4-dihydropyrimidine-2(1*H*)-thione group and to determine how conserved these interactions are upon substitution. To pursue these goals, molecular conformation analysis and detailed characterization of the intermolecular contacts were carried out on these four compounds as well as for eight other closely related structures found in CSD. Also, a comprehensive analysis of the intermolecular interactions was performed by applying a battery of complementary tools, including: (1) analysis of the topology of the electron density obtained from a periodic quantum calculation within the context of the Bader's theory of atoms in molecules (AIM)[15] to characterize the intermolecular interactions, (2) calculating the lattice energies and intermolecular interaction energies associated with different molecular pairs in order to determine the energy components contributing to crystal stabilization,[16,17] (3) using Hirshfeld-surface-based tools, such as d_{norm}, *Shape index* and *Curvedness* surface properties,[18,19] for exploration of the packing modes and for visualization of the intermolecular interactions, (4) obtaining quantitative pictures of the intermolecular contacts, including the relative percentage of each type of interaction, from fingerprint plots and studying their decompositions,[20,21] and (5) analyzing the intermolecular interactions in terms of a combined quantitative study based on the electrostatic potential (ESP) and on 3D deformation density maps.[22]

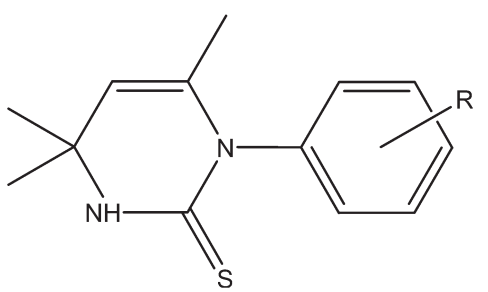

Scheme 1 General structure of 1-(*R*-phenyl)-4,4,6-trimethyl-3,4-dihydropyrimidine-2(1*H*)-thiones.

2 Experimental

2.1 Preparation of 1-(*R*-phenyl)-4,4,6-trimethyl-3,4-dihydropyrimidine-2(1*H*)-thione derivatives

In an attempt to obtain the corresponding acyl thiourea derivative, Yamin *et al.*[23,24] isolated 1-phenyl-4,4,6-trimethyl-3,4-dihydropyrimidine-2-(1*H*)thione from the reaction between cinnamoyl isothiocyanate and aniline in acetone. We demonstrated that 1-aryl-4,4,6-trimethyl-3,4-dihydropyrimidine-2-(1*H*)thiones are in fact formed by the reaction of aniline, KSCN, and 4-methylpent-3-en-2-one—an aldol condensation product of acetone formed *in situ* from the use of acetone as the solvent.[9,10,25] Following this general method, suitable substituted anilines (1.0 mmol) were added portion-wise to a stirred suspension of potassium thiocyanate (1.0 mmol) in 4-methylpent-3-en-2-one (1.20 mmol) at room temperature. The reaction mixture was heated at 50–60 °C for 3–5 h and the progress was followed by TLC. On completion, the reaction mixture was cooled to room temperature and poured into ice-water. The precipitated compounds were recrystallized from ethanol to afford the purified dihydropyrimidine-2-thiones (**1–4**) in good to excellent yields (Scheme 2).

1-(2-Chlorophenyl)-4,4,6-trimethyl-3,4-dihydropyrimidine-2(1*H*)-thione (1). White crystalline solid; yield; 92%, R_f: 0.31; m.p: 123–124 °C; IR (neat): 3390 (NH), 3029 (=C–H stretch), 1645 (CS–NH), 1576 (C=C), 1297 (C–N): ^{1}H-NMR ($CDCl_3$, 300 MHz): δ 7.88 (s, 1H, N–H), 7.22–6.45 (m, 5H, Ar–H), 4.25 (s, 1H, Csp^2–H), 1.41 (s, 3H, Csp^2–CH_3) 1.28 (s, 3H, CH_3), 1.24 (s, 3H, CH_3); ^{13}C-NMR ($CDCl_3$, 75 MHz): δ 187.5 (CSNH), 138.1 (–C=C–), 137.3, 135.2, 134.7, 131.7, 130.4, 129.8, 110.6 (–H–C=C–), 57.4 ($(CH_3)_2$–C–), 34.2 ($(CH_3)_2$–), 33.4 (–C–CH_3). Elemental analysis $C_{13}H_{15}ClN_2S$: calc (%): C 58.97, H 5.23, Cl 13.26, N 10.54, S 12.01; found (%): C 58.94, H 5.27, Cl 13.28, N 10.53, S 12.00.

1-(2,3-Di-chlorophenyl)-4,4,6-trimethyl-3,4-dihydropyrimidine-2(1*H*)-thione (2). Brown crystalline solid; yield; 81%, R_f: 0.33; m.p: 130–131 °C; IR (neat): 3401 (NH), 3087 (=C–H stretch), 1694 (CS–NH), 1598 (C=C), 1307 (C–N): ^{1}H-NMR ($(CD_3)_2CO$, 300 MHz): δ 7.99 (s, 1H, N–H), 7.64–7.29 (m, 5H, Ar–H), 5.04 (q, 1H, J = 1.2 Hz, Csp^2–H), 1.52 (d, 3H, J = 1.2 Hz, Csp^2–CH_3) 1.44–1.41 (s, 6H, 2 × CH_3); ^{13}C-NMR ($(CD_3)_2CO$, 75 MHz): δ 183.1 (CSNH), 137.5 (–C=C–), 137.1, 135.9, 132.8, 128.5, 128.1, 127.6, 107.9 (–H–C=C–), 57.1 ($(CH_3)_2$–C–), 33.6 [$(CH_3)_2$–], 32.7 (–C–CH_3). GC-MS: 300 (M^+), 285, 265 (100%), 249, 226, 185. Elemental analysis $C_{13}H_{14}Cl_2N_2S$: calc (%): C 51.95, H 4.56, Cl 23.50, N 9.33, S 10.65; found (%): C 51.98, H 4.53, Cl 23.54, N 9.31, S 10.63.

1-(2,4-Dimethylphenyl)-4,4,6-trimethyl-3,4-dihydropyrimidine-2(1*H*)-thione (3). White crystalline solid; yield; 85%, R_f: 0.32; m.p: 150–151 °C; IR (neat): 3320 (NH), 3082 (=C–H stretch), 1697 (CS–NH), 1535 (C=C), 1290 (C–N): ^{1}H-NMR ($(CD_3)_2CO$, 300 MHz): δ 7.72 (s, 1H, N–H), 7.08–6.89 (m, 3H, Ar–H), 4.97 (q, 1H, J = 1.2 Hz, Csp^2–H), 2.31 (s, 3H, Ar–CH_3), 2.17 (s, 3H, Ar–CH_3), 1.44 (d, 3H, J = 1.2 Hz, Csp^2–CH_3), 1.39 (6H, 2 × CH_3); ^{13}CNMR ($(CD_3)_2CO$, 75

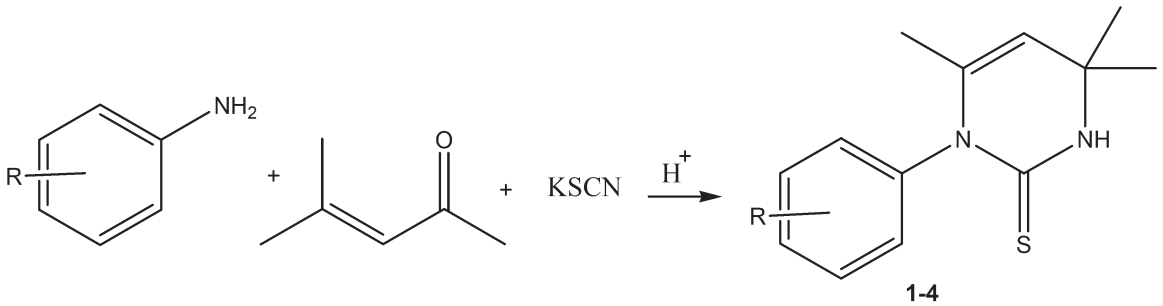

R= 2-Cl (**1**), 2,3-Cl_2 (**2**), 2,4-(CH_3) (**3**), 4-MeO (**4**)

Scheme 2 Green synthesis of 1-(*R*-phenyl)-4,4,6-trimethyl-3,4-dihydropyrimidine-2(1*H*)-thiones **1**–**4**.

MHz): δ 177.2 (CSNH), 138.1 (–C═C–), 137.5, 136.5, 131.8, 130.8, 129.9, 128.8, 109.2 (–H–C═C–), 51.8 ($(CH_3)_2$–), 30.8 ($(CH_3)_2$–C–), 20.2 (–C–CH_3), 19.6 (2 × Ar–CH_3): GC-MS: 260 (M^+), 245 (100%), 179, 163, 79. Elemental analysis $C_{15}H_{20}N_2S$: calc (%): C 69.14, H 7.79, N 10.72, S 12.35; found (%): C 69.17, H 7.75, N 10.71, S 12.37.

1-(4-Methoxyphenyl)-4,4,6-trimethyl-3,4-dihydropyrimidine-2(1*H*)-thione (4). Red crystalline solid; yield; 87%, R_f: 0.47; m. p: 163–164 °C; IR (neat): 3355 (NH), 3045 (═C–H stretch), 1700 (CS–NH), 1585 (C═C), 1301 (C–N): ^{1}H-NMR ($CDCl_3$, 300 MHz): δ 7.81 (s, 1H, N–H), 7.65–6.17 (m, 5H, Ar–H), 4.61 (s, 1H, Csp^2–H), 3.71 (s, 3H, Ar–OCH_3), 1.64 (s, 3H, Csp^2–CH_3) 1.24 (s, 3H, CH_3), 1.21 (s, 3H, CH_3); ^{13}C-NMR ($CDCl_3$, 75 MHz): δ 186.5 (CSNH), 137.9 (–C═C–), 134.7, 126.3, 121.9, 120.2, 111.2 (–H–C═C–), 57.9 ($(CH_3)_2$–C–), 54.6 (Ar–OCH_3), 33.8 ($(CH_3)_2$–), 32.4 (–C–CH_3). LC-MS (*m*/*z*) %: $[M + H]^+$ 263.6 (100%). Elemental analysis $C_{14}H_{18}N_2OS$: calc (%): C 64.05, H 6.96, N 10.64, O 6.15, S 12.21; found (%): C 64.03, H 6.93, N 10.66, O 6.16, S 12.20.

Instrumentation. The melting points were determined using a Gallenkamp melting point apparatus (MP-D) and are presented herein uncorrected. Infrared spectra were recorded using a Shimadzu IR 460 as KBr pellets. ^{1}H-NMR spectra were obtained using a Bruker 300 NMR MHz spectrometer in deuterated solvents using TMS as an internal reference. ^{13}CNMR spectra were obtained by a (75 MHz) NMR spectrometer in deuterated solvents. MS were recorded using an EI source (70 eV) on Agilent Technologies 6890N (GC) and an inert mass selective detector 5973 mass spectrometer. Gaseous helium was used as the mobile phase with the pressure in the column head equal to 100 kPa. The column used was a 19091J-433 HP-5 of 30 m × 0.32 mm × 0.25 mm film thickness. Approximately 1 μL volume of the compounds dissolved in $CHCl_3$ or acetone were chromatographed under the following conditions: the injection temperature was 200 °C, the initial column temperature (70 °C) was held for 2 min, then increased to 200 °C at 10 °C min^{-1}, and held for 4 min after elevation to 250 °C at 10 °C min^{-1} and held for 2 min more. In the spectrometer, the source was kept at 200 °C. Thin layer chromatography (TLC) was conducted on 0.25 mm silica gel plates (60 F254, Merck). Elemental analyses were conducted using the CHNS 932 LECO instrument.

X-ray data collection and structure refinement. The crystal and refinement data for compounds **1**–**4** are listed in Table 1. Data were collected at 130(2) K on a Bruker AXS SMART APEX diffractometer using MoKα radiation. The structures were solved by direct methods and full-matrix least-squares refinement on F^2 by using SHELX.[26] All the non-hydrogen atoms were refined anisotropically, while all the H atoms were derived from difference maps, then placed at idealized positions, and then refined using the riding model. Methyl-H atoms were allowed to rotate but not to tip. The ring puckering parameters and geometric parameters of π-stacking were calculated with PLATON for Windows Taskbar v1.17.[27] The molecular structures were plotted using Olex2,[28] and the packing diagrams were generated using MERCURY.[29]

Full crystallographic data have been deposited with the Cambridge Crystallographic Data Centre (CCDC-1504146, 1504147, 1504148, 1504149 for **1**–**4**, respectively).

Topological analysis. Periodic calculations were performed at the B3LYP/6-31G(d,p) level with the Crystal14 code.[30] Using the experimental estimations as the starting point, the coordinates of the hydrogen atoms in the crystal were optimized to minimize the B3LYP/6-31G** crystal energy, with heavy atom coordinates and cell parameters fixed at their experimental values. The topology of the resulting electron density was then analyzed using the TOPOND14 code.[31,32] For consistency with the periodic results, molecular and supramolecular electron densities were also analyzed with TOPOND98 from calculations performed with Crystal98 using a geometry optimized with Crystal09.

Lattice and interaction energies. Lattice energy and intermolecular interaction energies for specific molecular pairs were calculated using the CLP (Coulomb–London–Pauli) approach implemented in the PIXEL program package.[33,34]

Hirshfeld surface calculations. Hirshfeld surfaces and their associated two-dimensional (2D) fingerprint plots[35–38] were plotted using *CrystalExplorer*3.0 software.[39] The d_{norm} (normalized contact distance) surface and the breakdown of the 2D fingerprint plots were used for decoding and quantifying the intermolecular interactions in the crystal lattice. The fingerprint plots could be decomposed to highlight particular atom pair close contacts[40] that overlap in the full fingerprint. The d_{norm} is a symmetric function of the distances to the

Table 1 Crystal data and structure refinement for compounds **1–4**

	(1)	(2)	(3)	(4)
Empirical formula	$C_{13}H_{15}ClN_2S$	$C_{13}H_{14}Cl_2N_2S$	$C_{15}H_{20}N_2S$	$C_{14}H_{18}N_2OS$
Formula weight	266.78	301.22	260.39	262.36
Temperature/K	130(2)	130(2)	130(2)	130(2)
Crystal system	Monoclinic	Monoclinic	Monoclinic	Triclinic
Space group	$P2_1/c$	$P2_1/c$	$P2_1/n$	$P\bar{1}$
Unit cell dimensions	a = 14.214(2) Å	a = 12.072(4) Å	a = 12.228(3) Å	a = 8.729(3) Å
	b = 9.8017(14) Å	b = 7.010(2) Å	b = 8.896(2) Å	b = 9.683(3) Å
	c = 19.392(3) Å	c = 17.035(5) Å	c = 14.798(4) Å	c = 10.503(4) Å
				α = 64.578(5)°
	β = 95.548(4)°	β = 101.402(7)°	β = 113.166(6)°	β = 78.685(6)°
				γ = 63.892(6)°
Volume/Å^3	2689.0(7)	1413.2(7)	1480.1(6)	719.9(4)
Z	8	4	4	2
$\rho_{calc.}$/mg mm^{-3}	1.318	1.416	1.169	1.210
μ/mm^{-1}	0.419	0.520	0.204	0.216
F(000)	1120	624	560	280
Crystal size/mm^3	0.32 × 0.16 × 0.12	0.23 × 0.11 × 0.04	0.38 × 0.06 × 0.03	0.48 × 0.21 × 0.04
Theta range for data collection	1.44 to 27.87°	1.72 to 27.88°	1.84 to 27.88°	2.15 to 27.10°
Index ranges	$-18 \le h \le 18$	$-15 \le h \le 15$	$-15 \le h \le 16$	$-11 \le h \le 8$
	$-12 \le k \le 12$	$-9 \le k \le 9$	$-11 \le k \le 11$	$-12 \le k \le 11$
	$-25 \le l \le 25$	$-22 \le l \le 21$	$-19 \le l \le 18$	$-13 \le l \le 13$
Reflections collected	24 935	12 844	13 456	5079
Independent reflections	6406 [$R_{(int)}$ = 0.057]	3377 [$R_{(int)}$ = 0.089]	3524 [$R_{(int)}$ = 0.100]	3133 [$R_{(int)}$ = 0.067]
Data/restraints/parameters	6406/0/309	3377/0/164	3524/0/168	3133/0/167
Goodness-of-fit on F^2	0.934	1.008	0.765	0.824
Final R indexes [$I > 2\sigma(I)$]	R_1 = 0.0499	R_1 = 0.0537	R_1 = 0.0544	R_1 = 0.0522
	wR_2 = 0.1064	wR_2 = 0.1075	wR_2 = 0.0865	wR_2 = 0.0852
Largest diff. peak/hole/e Å^{-3}	0.569/−0.379	0.563/−0.371	0.376/−0.327	0.241/−0.268

surface from nuclei inside and outside the Hirshfeld surface (d_i and d_e, respectively), relative to their respective van der Waals radii. The 3D d_{norm} surfaces were mapped over a fixed color scale of −0.135 au (red) to 0.460 Å au (blue). The 2D fingerprint plots were displayed by using the translated 0.6–2.6 Å range, and included reciprocal contacts. Electrostatic potentials on 0.008 e au^{-3} isosurfaces were calculated at the HF/6-31G* level by using the Tonto program[41] integrated into *CrystalExplorer*. 3D-deformation densities were plotted over the electron density isosurface (0.008 e au^{-3}), with charge depleted (CD) and charge concentrated (CC) regions colored in red and blue, respectively.

The similarity/dissimilarity between the structures was evaluated using XPac2.0,[42] which allows identifying and comparing "supramolecular constructs" (SCs) for pairs of structures with the same space group and similar cell dimensions. The SCs are sub-components of complete crystal structures of 0D, 1D (a row of molecules match), 2D (a layer of molecules match), and 3D similarity (isostructural systems). Furthermore, the XPac method establishes the dissimilarity index 'x' and the stretch parameter D as a measure of how far two crystal structures differ from perfect geometrical similarity.

3 Results

3.1 Conformational analysis

The molecular structures for compounds **1–4** are shown in Fig. 1. In compound **1**, there are two independent molecules (A and B) in the asymmetric unit. An overlay diagram of the molecules shows that molecule A is virtually super-imposable upon molecule B (Fig. S1, ESI†), and the *r.m.s* deviations with and without inversion are 1.712 and 0.54 Å, respectively, matching all the non-H atoms. The major difference between the matched molecules is found in the twist of the axial-CH_3 with respect to the C–Cl group, with the C107–C101···C114–Cl1 and C207–C201···C214–Cl2 pseudo-torsion angles being −172.8(2) and −3.4(2)° for molecules A and B, respectively. These results indicate that the axial-CH_3 and C–Cl groups lie on opposite sides of the heterocyclic plane in molecule A, while they are on the same side in molecule B.

In all the structures, the rings are twisted around each other around the N2–C(Ph) bond. The mean planes of the heterocyclic rings through four coplanar atoms make dihedral angles of 87.0(1)° (average), 85.4(1)°, 87.7(1)°, and 83.6(1)° with the benzene ring for compounds **1–4**, respectively, as found in other families of 3,4-dihydropyrimidine-2(1*H*)-thione/one derivatives.[43,44] However, the benzene ring is equatorial in structures **1–4**, and axial in the referred compounds,[43,44] leading to extended and folded molecular conformations, respectively.

The ring puckering parameters[45] and the endocyclic torsion angles for the pyrimidine ring are shown in Tables S1 and S2 (ESI†).

3.2 Crystal structures: a topological description

A brief description of the crystal structures of compounds **1–4** based on the main close shell interactions characterized

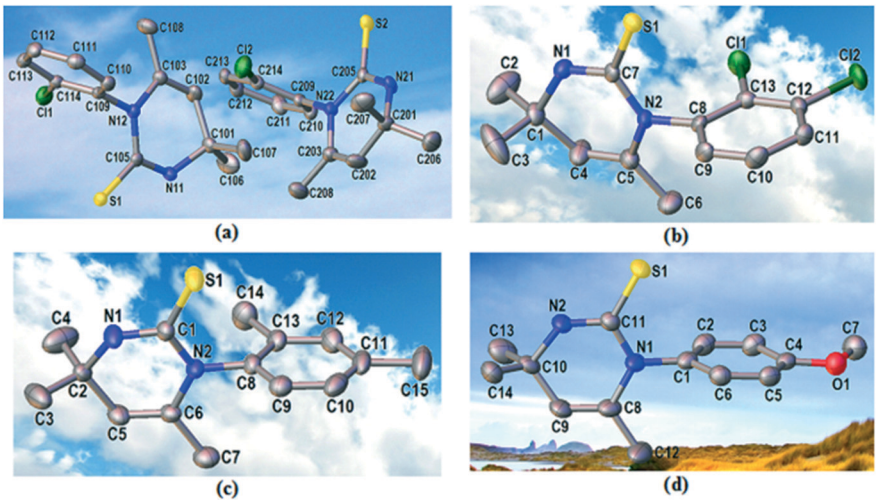

Fig. 1 Views of the molecular structures for 1-(*R*-phenyl)-4,4,6-trimethyl-3,4-dihydropyrimidine-2(1*H*)-thione derivatives, (a) *R* = 2-chloro, with two independent molecules A and B, (b) *R* = 2,3-dichloro, (c) *R* = 2,4-dimethyl and (d) *R* = 4-methoxy. Displacement ellipsoids are drawn at the 50% probability level. Atoms numbering are given, while the H atoms are omitted for clarity.

from AIM topological analysis of the corresponding electron densities follows. The strategy consists in associating substructures of growing dimensionality with interactions of decreasing strength, using for this respect a criterion based on the values at the critical point of the electron density and on the positive curvature of the Laplacian.[46]

The basic structural block in compound **1** is set up from two molecules that are linked through two N–H···S interactions (I and II in Table S3, ESI,† and Fig. 2), these being the most relevant from the topological viewpoint. The computed H···S distances and N–H···S angles are 2.42/2.60 Å and 161°/146° for the two molecules (A/B) within the asymmetric unit,

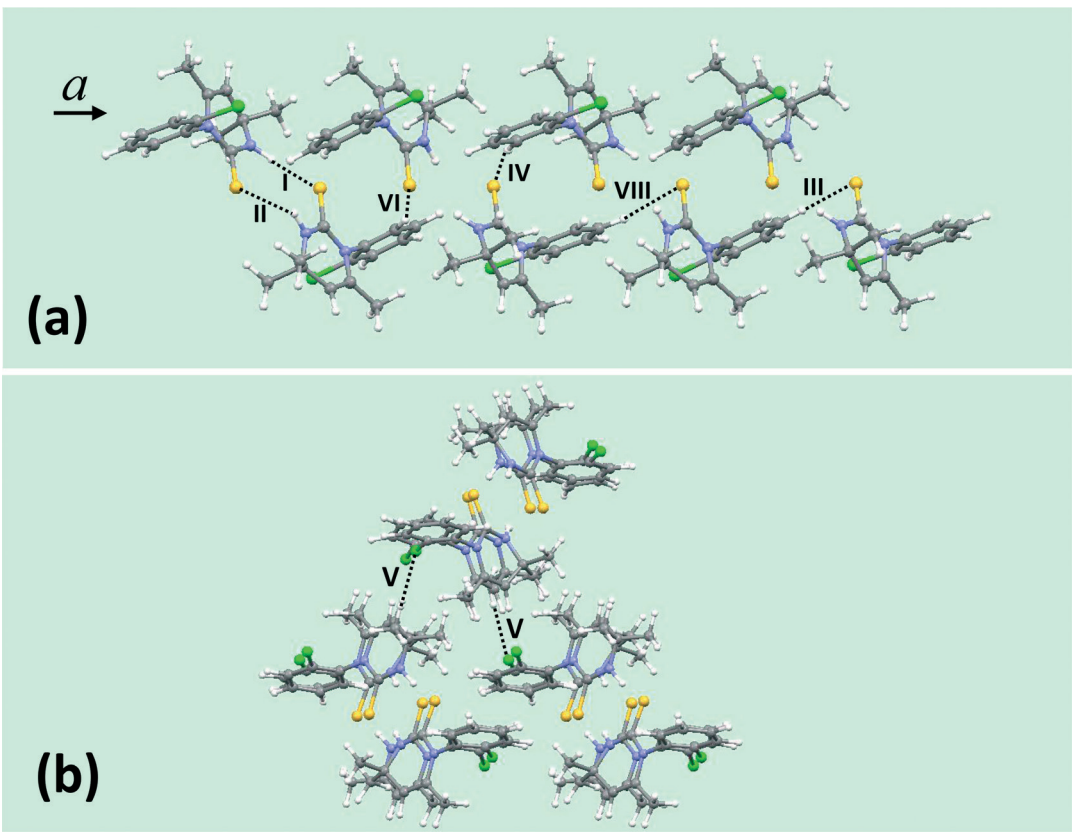

Fig. 2 (a) Chain of pseudo-centrosymmetric pairs of molecules along the *a* axis direction; (b) consecutive shackles of three chains in the crystal structure of compound **1**.

respectively (see Table S3†), which are in qualitative good agreement with the experimental data (2.54/2.71 Å and 162°/147°). Molecules in the pair are also linked to each other by a $H_{me}\cdots S$ interaction (VII). Connections between the pairs through four $S\cdots H_R$ interactions (III, IV, VI, and VIII) give rise to infinite chains along the *a* axis direction (see Fig. 2). $Cl\cdots H_{me}$ interactions (V) acting between the chains in two different directions complete the main 3D interaction network.

In compound **2**, the molecules are linked through one N–H···S, two $H_R\cdots S$, and one $H_{me}\cdots S$ interaction (I, II, III, and IV in Table S4, ESI,† and Fig. 3), giving rise to infinite chains along the *b* axis direction. Chains linked to each other through pairs of $H_{me}\cdots S$ interactions (VI in Table S3, ESI,† and Fig. 3) form layers parallel to (1 0 0). The main 3D interaction network is completed by Cl2···Cl2 interactions (V) connecting the layers to each other (see Fig. 3). The computed $d_{Cl\cdots Cl}$ distance is 3.38 Å, which is in perfect agreement with the experimental value.

The basic structural blocks of compound **3** are centrosymmetric molecular pairs, with molecules linked through a pair of rather strong N–H···S interactions, geometrically characterized by $d_{H\cdots S}$ and $\theta_{D-H\cdots S}$ of 2.37 Å and 164°, respectively (I in Table S5 ESI,† and Fig. 4). Molecules in a pair are also linked to each other by a pair of $H_{me}\cdots S$ interactions (IV). The connections between molecular pairs through pairs of $S\cdots H_R$ interactions (II) give rise to infinite chains along [1 $\bar{1}$ 1] (see Fig. 4). On the other hand, a second set of $S\cdots H_R$ interactions (III) link centrosymmetric pairs in infinite chains along the *b* axis direction. A combination of the two chain kinds originates in layers parallel to ($\bar{2}$ 0 2).

For compound **4**, the basic substructures are also the centrosymmetric molecular pairs, with molecules linked through a pair of NH···S interactions (computed $d_{H\cdots S}$ and $\theta_{D-H\cdots S}$ values are 2.42 Å and 159°, respectively, see I in Table S6, ESI,† and Fig. 5). Connections between such molecular pairs through pairs of $O\cdots H_{me}$ interactions (II) give rise to infinite chains along the *a* axis direction (see Fig. 5). Pairs of $S\cdots H_R$ interactions (III) link chains to each other originating in layers parallel to (0 0 1). Connection between neighboring layers through $O\cdots H_{me}$ interactions (IV) completes the main 3D interaction network.

3.3 Structural motifs and interaction energies

For each crystal under consideration, the lattice energy and intermolecular interaction energies for specific molecular pairs were calculated using the CLP (Coulomb–London–Pauli) approach, which enables partitioning of the total energy into their Coulombic, polarization, dispersion, and repulsion contributions. These results are summarized in Table 2.

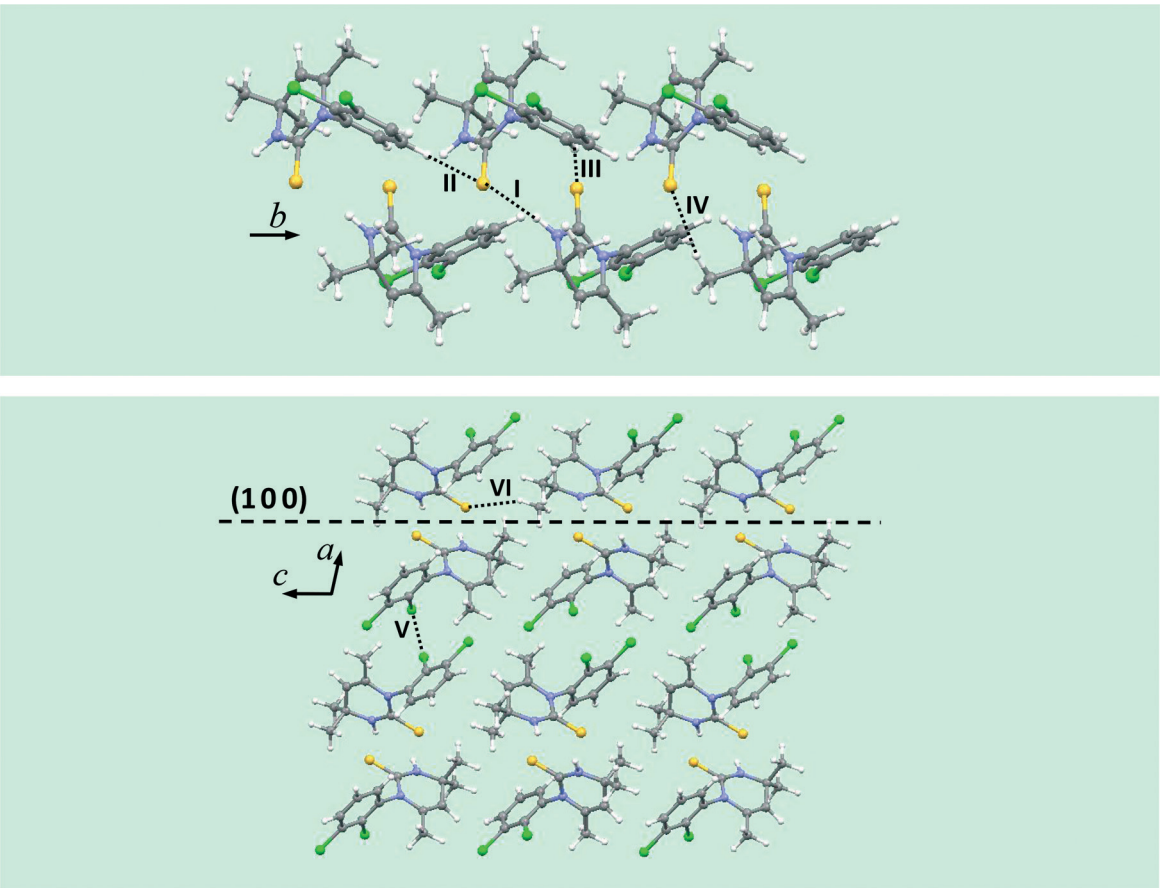

Fig. 3 *b* axis direction view of a chain (upper panel); and *b* axis direction view of two layers (lower panel) for compound **2**.

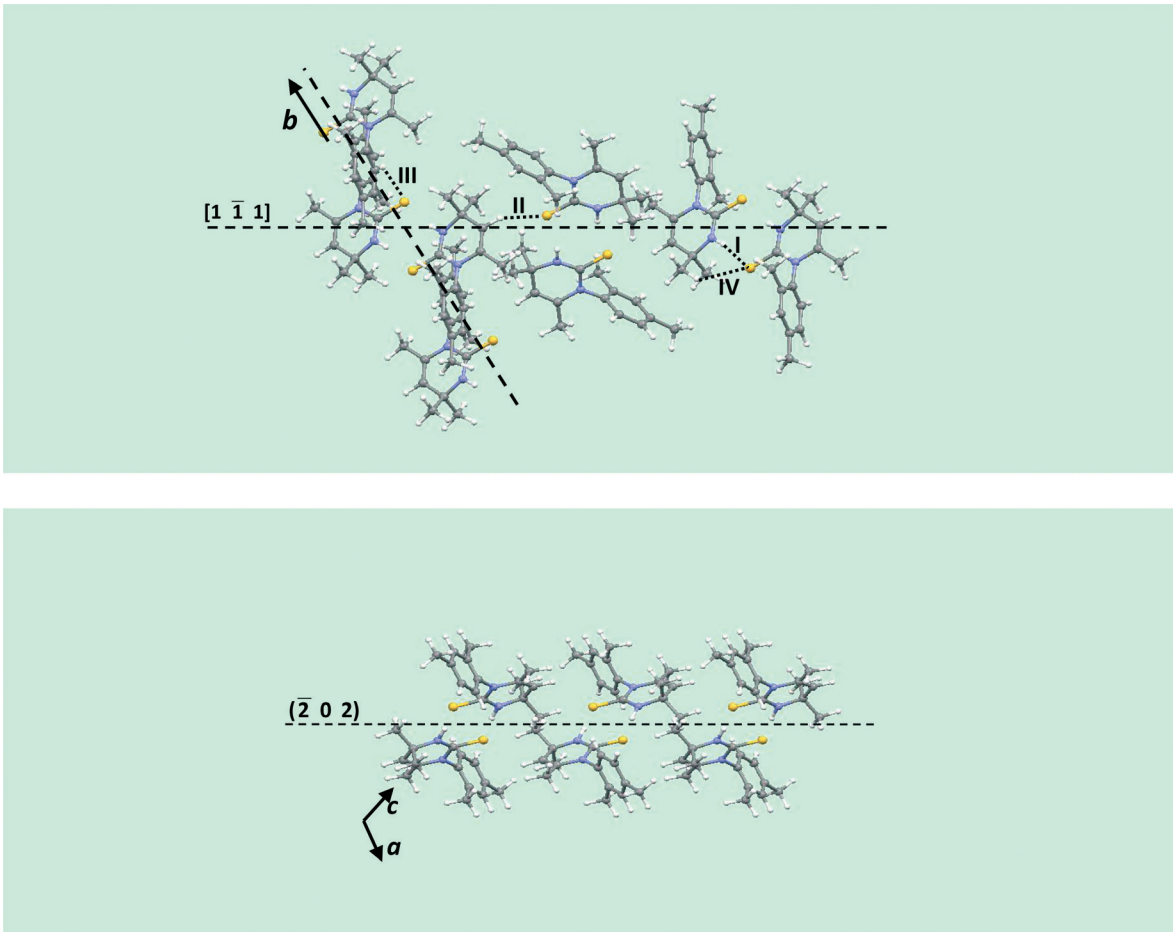

Fig. 4 View along a direction perpendicular to ($\bar{2}$ 0 2) of infinite chains along [1 $\bar{1}$ 1] and along the *b* axis (upper panel); and layer view along the *b* axis direction (lower panel) for compound **3**.

Detailed diagrams of the crystal packing for structures **1–4** are shown in Fig. S2–S5 (ESI†), respectively, and the geometries of the relevant intermolecular hydrogen bonds are listed in Table 3 (column 4) following the distance criteria[47] for the crystal packing analysis of a supramolecular motif. In order to compare the packing modes of **1–4** with similar structures, a search of the crystal structural database (CSD,[48] ConQuest 1.19 (ref. 49)) for the 4,4,6-trimethyl-3,4-dihydropyrimidine-2(1*H*)-thione moiety was undertaken, yielding eight hits: two structures corresponding to the *meta* (IJUGEA)[50,51] and *para* (DUNZIW)[9] isomers of compound **1**; another two related structures containing mono-substituents fluorine (EVEWIM)[52] and bromine (VAGSUR)[53] on the phenyl ring, two structures that are the *ortho*-methyl (IMARIY)[25] and *meta*-methyl isomers (PUJYID),[10] and structures related to the unsubstituted compound, which is present as orthorhombic (FAXVOQ-I)[23] and triclinic (FAXVOQ-II)[24] polymorphs. Relevant data for these structures are also included in Table 3.

3.4 Hirshfeld surface analysis

For a better comprehension of the crystal packing for compounds **1–4**, a complete description of the main intermolecular interactions using Hirshfeld surface analysis was carried out. Fig. 6 shows surfaces mapped over the d_{norm} property in a similar orientation. The surfaces are shown as transparent to allow visualization of the molecules. Contacts with distances equal to the sum of the van der Waals radii are represented as white regions, while the contacts with distances shorter than and longer than van der Waals radii are shown as red and blue colors, respectively.

A close examination with *Shape index* and *Curvedness*, which are the Hirshfeld surface properties generally used to identify planar stacking arrangements,[37] was performed. The pattern of touching red and blue triangles on the *Shape index* surfaces is characteristic of π–π stacking.[37] This type of interaction is also evident as relatively large and green flat regions delineated by blue circles on the corresponding *Curvedness* surfaces.[40]

The full 2D fingerprint plots and decomposed fingerprint plots of the main intermolecular interactions are depicted in Fig. 7, while the relative contributions of the individual intermolecular interactions to the Hirshfeld surface area of structures **1–4** and full 2D fingerprint plots for eight related compounds are shown in Fig. S7 and S8, respectively (ESI†). For IJUGEA, our data are in close agreement with the Hirshfeld surface analysis recently reported by Babashkina *et al.*[51]

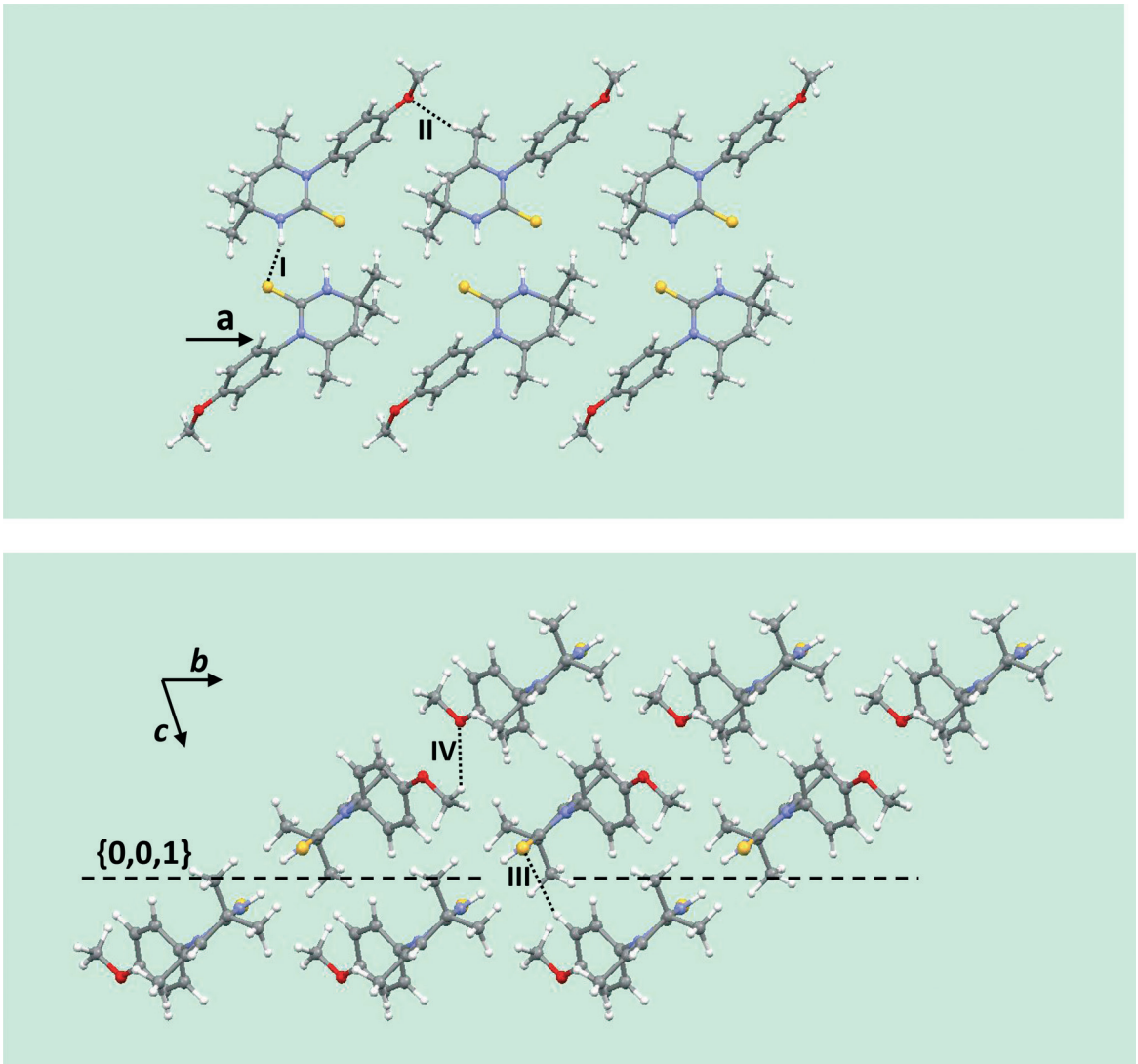

Fig. 5 Infinite chain along the *a* axis direction (upper panel); and layer view along the *a* axis direction (lower panel) for compound **4**.

3.5 Electrostatic potential and 3D deformation density

The surprising energy results about the relevance of the Coulombic contributions found in the studied structures prompted us to enhance the study of the intermolecular interactions by analyzing the electrostatic potential (ESP) maps.[54] Consequently, the ESP maps of compounds **1**–**4** are presented in Fig. S9a–S12a in the ESI,† and the magnitudes of the electrostatic potentials for all 12 structures are given in Table S8 (ESI†). In general, the ESP maps show an asymmetric charge distribution in the molecules, generating relevant polarization effects as reflected by high dipole moments ranging from 4.87 D for VAGSUR to 5.86 D for compound **3** (Table S8†).

Table 2 Lattice energies (kJ mol^{-1}) partitioned into Coulombic (E_{coul}), polarization (E_{pol}), dispersion (E_{disp}), and repulsion (E_{rep}) components for **1**–**4** and related compounds

Compound	E_{coul}	E_{pol}	E_{disp}	E_{rep}	E_{TOT}
1	−75.6	−38.2	−148.6	124.7	−137.7
2	−71.1	−38.9	−161.3	121.8	−149.4
3	−72.2	−40.6	−138.2	115.3	−135.7
4	−86.4	−41.4	−143.8	123.1	−148.4
IJUGEA	−82.1	−40.5	−151.8	130.3	−144.2
DUNZIW	−74.8	−40.6	−154.1	122.8	−146.7
EVEWIM	−66.3	−32.7	−119.0	91.7	−126.2
VAGSUR	−68.9	−37.7	−127.3	102.2	−131.8
IMARIY	−74.3	−41.8	−133.1	116.0	−133.1
PUJYID	−66.7	−35.5	−141.5	110.7	−133.0
FAXVOQ-I	−69.9	−35.5	−130.8	105.0	−131.3
FAXVOQ-II	−65.3	−29.8	−132.2	97.5	−129.8

4 Discussion

The dihydropyrimidine-2(1*H*)-thione rings of the studied species adopt a puckered conformation, and a description based on the canonical conformations for six-membered rings is given. In structure **1** (Mol. A), the pyrimidine ring adopts an intermediate conformation between an ^{2}E and $^{2}S_{1}$ screw-boat form, whereas in structures **1** (Mol. B) and **2**, an E_{2} envelope

Table 3 Interaction energies (E_{TOT}) partitioned into Coulombic, polarization, dispersion, and repulsion contributions (kJ mol^{-1}) for various molecular pairs in **1**–**4** and related compounds

Compound	Symmetry	Involved interactions	d(H···A), ∠D—H···A	Centroid distance	E_{coul}	E_{pol}	E_{disp}	E_{rep}	E_{TOT}
1	$x, \frac{1}{2}-y, -\frac{1}{2}+z$	N11–H1A···S2,	2.539(1), 162	7.534	−66.5	−38.4	−38.1	74.8	−68.2
		N21–H2A···S1	2.707(1), 147						
	$-x, 1-y, 1-z$	C110–H11A···S1	2.901(1), 168	5.774	−28.4	−17.6	−44.4	42.6	−47.8
	$x, -1+y, z$	C207–H20G···Cl1	2.788(1), 172	8.532	−6.2	−3.2	−20.4	14.0	−15.9
	$-x, 2-y, 1-z$	Cg···Cg	4.104(1)[a]	7.746	−25.0	−9.5	−38.0	29.5	−43.0
2	$-x, -\frac{1}{2}+y, \frac{1}{2}-z$	N1–H1A···S1,	2.65(2), 163	7.135	−45.0	−25.5	−40.7	50.2	−61.0
		C9–H9A···S1	2.931(1), 161						
	$1-x, \frac{1}{2}+y, \frac{1}{2}-z$	C6–H6C···Cl1	3.179(1), 128	6.841	−5.0	−2.5	−32.7	14.8	−25.4
	$1-x, -\frac{1}{2}+y, \frac{1}{2}-z$	Cl1···C12	3.985(1)[b]	6.841	−5.0	−2.5	−32.7	14.8	−25.4
	$1-x, 1-y, -z$	Cl2···Cl2	3.381(2)[c]	11.536	−2.8	−1.6	−8.8	9.1	−4.1
3	$1-x, 2-y, 2-z$	N1–H1A···S1	2.48 (2), 164	7.781	−80.7	−52.2	−40.1	94.3	−78.7
	$-\frac{1}{2}+x, 1.5-y, -\frac{1}{2}+z$	C5–H5A···S1	2.989(1), 128	7.606	−14.1	−8.0	−28.4	22.4	−28.2
4	$-x, 2-y, -z$	N2–H2···S1	2.529(1), 160	8.154	−79.1	−47.0	−39.5	87.5	−78.0
	$1-x, 1-y, -z$	C3–H3A···S1	2.929(1), 154	6.043	−28.1	−14.4	−40.4	34.5	−48.5
	$-1+x, y, z$	C12–H12A···O1	2.47(1), 154	8.729	−15.0	−5.7	−24.8	17.7	−27.8
	$2-x, -y, 1-z$	C7–H7B···O1	2.671(2), 130	12.869	−6.7	−2.5	−10.8	8.7	−11.2
IJUGEA	$2-x, 2-y, 1-z$	N1–H1A···S1	2.583(1), 162	7.944	−73.6	−43.2	−38.1	81.3	−73.6
	$1-x, 2-y, -z$	C9–H9···Cl1	3.021(1), 120	5.773	−27.6	−14.1	−46.9	41.6	−47.0
DUNZIW	$1-x, y, \frac{1}{2}-z$	N3–H1···S1	2.59(3), 169	8.299	−68.4	−45.0	−37.5	79.9	−71.0
	$1.5-x, 1.5-y, 2-z$	C15–H15···Cl1	3.049(1), 158	11.476	−3.0	−1.8	−12.7	7.5	−10.0
EVEWIM	$1-x, -y, 1-z$	N1–H1A···S1	2.571(1), 162	7.628	−69.8	−41.2	−36.5	77.4	−70.0
	$-1+x, y, z$	C3–H3A···F1	2.649(2), 153	8.814	−8.5	−2.6	−15.1	7.5	−18.7
VAGSUR	$-x, -y, -z$	N2–H1···S1	2.426(3), 170	7.920	−75.4	−48.7	−38.5	87.4	−75.1
	$x, \frac{1}{2}-y, \frac{1}{2}+z$	C5–H8···S1	2.981(3), 127	7.501	−13.3	−7.2	−27.1	20.6	−27.1
	$1-x, \frac{1}{2}+y, \frac{1}{2}-z$	C7–H11···Br1	3.072(2), 123	6.689	−3.6	−1.7	−24.2	11.2	−18.3
IMARIY	$1-x, 1-y, -z$	N2–H2···S1	2.54(3), 169	7.347	−80.4	−52.8	−39.6	94.6	−78.1
	$\frac{1}{2}+x, \frac{1}{2}-y, \frac{1}{2}+z$	C9–H9A···S1	2.938(1), 130	7.586	−15.6	−8.3	−27.5	24.5	−26.8
PUJYID	x, y, z	N1–H1N···S2	2.621(1), 151	7.528	−61.4	−40.2	−37.1	72.5	−66.2
		N3–H3N···S1	2.596(1), 163						
FAXVOQ-I	x, y, z	N2–H2A···S2	2.608(1), 158	7.292	−66.5	−38.9	−35.5	69.1	−71.7
		N4–H4A···S1	2.636(1), 167						
	$\frac{1}{2}+x, y, \frac{1}{2}-z$	C12–H12A···S1	2.968(1), 155	5.063	−22.8	−13.5	−52.5	43.4	−45.5
FAXVOQ-II	$1-x, 1-y, 2-z$	N2–H2A···S1	2.707(1), 148	7.256	−61.4	−31.5	−36.6	64.3	−65.2
	$x, -1+y, z$	C13–H13A···S1	2.921(1), 166	8.649	−10.2	−4.8	−17.7	12.7	−20.1

[a] Inter-centroid distance, Cg is the centroid of the C109–C114 ring; [b] Cl···C distance; [c] Cl···Cl distance.

conformation with C101 and C1 atoms as flap atoms, respectively, is adopted. In compound **3**, the heterocyclic ring adopts a conformation which can best be described as an intermediate between a $^6S_1$ screw-boat and an $^6H_1$ half-chair form. An E_4 envelope with its apex at the C10 atom was observed for structure **4**. The validity of these descriptions is borne out by the corresponding endocyclic torsion angles (Table S2, ESI†). The thionyl and 4-methyl groups all have equatorial orientations, while the two 6-methyl groups present pseudo-equatorial orientations.

The similarity/dissimilarity between the 12 closely related structures was quantitatively analyzed.[55] The pair of *ortho*-substituted VAGSUR/IMARIY compounds revealed the presence of 3D-SC, showing a high degree of isostructurality, as reflected by the 'x' and D values of 2.6 and 0.13 Å, respectively. The similarity/dissimilarity was also examined for the pairs **3**/IMARIY and **3**/VAGSUR structures, which showed SC with a minor but similar degree of isostructurality, as reflected by the ('x', D) values of (8.2, 0.49 Å) and (8.4, 0.36 Å), respectively. In spite of having the same space group and relatively similar cell dimensions for the PUJYID and FAXVOQ-I structures, no significant structural similarity was found in this pair of compounds. No other pair of compounds presented isostructurality.

The topological analysis of the electron densities highlighted the preponderance of N–H···S interactions in the stabilization of the crystal packing of the whole series of compounds studied herein. In compound **1**, two N–H···S interactions were observed for the two independent molecules in the asymmetric unit. For compounds **3** and **4**, centrosymmetric molecular pairs were observed, with molecules linked through such a pair of N–H···S interactions. Furthermore, non-classical H_{me}···S and S···H_R were significant contributors in the stabilization of the dihydropyrimidine-2(1*H*)-thione synthon, as observed for compounds **1**–**4**, while Cl···H_{me} and Cl···Cl were also observed for the chlorinated species **1** and **2**.

The lattice energy values (Table 2) showed that the dispersion energy (E_{disp}) was the major contribution toward the crystal stabilization for all the compounds as generally

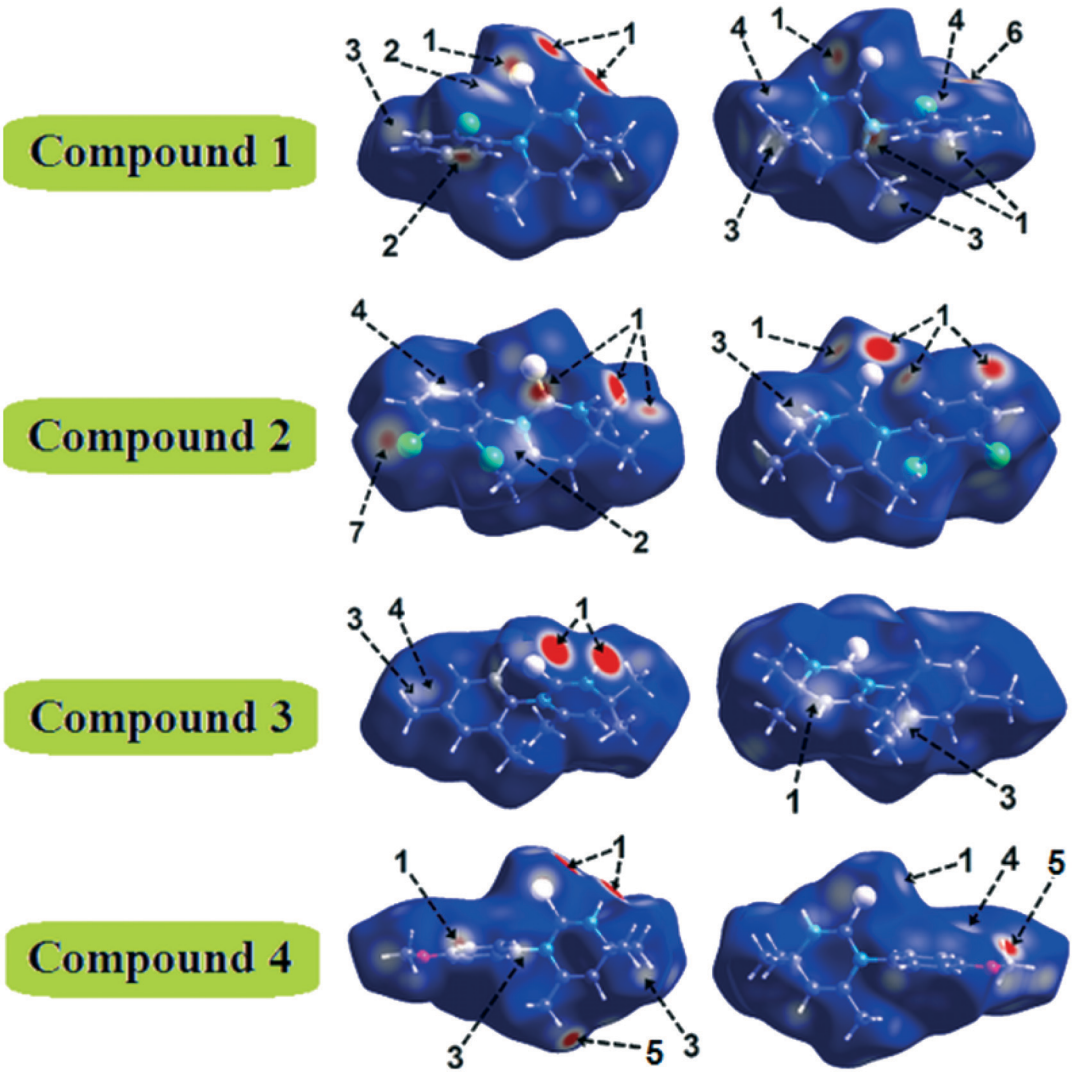

Fig. 6 Views of the Hirshfeld surfaces mapped with d_{norm} in two orientations: front view and back view (180° rotated around the vertical axis of the plot). Close contacts are labeled as follows: (1) S···H, (2) Cl···H, (3) H···H, (4) C···H, (5) O···H, (6) C···C, and (7) Cl···Cl.

expected for organic species, with similar percentages ranging from 53.0% in compound **4** to 59.5% in compound **2**. However, the Coulombic component (E_{coul}) was very significant for all the structures, representing the second highest contributor, ranging from 26.2% (compound **2**) to 31.8% (compound **4**). A complementary description was obtained when the results of the intermolecular energy calculations for selected molecular pairs were considered, as shown in Table 3. The occurrence of N–H···S hydrogen bonds forming $R_2^2(8)$ motifs was a common feature for all the structures, except in compound **2** (Fig. S2 and S3, ESI†), generating molecular pairs with the highest energy stabilization (from −78.7 kJ mol^{-1} for compound **3** to −61.0 kJ mol^{-1} for compound **2**) in comparison with molecular pairs involving other types of contacts. PIXEL energies also revealed that the highest contribution toward the crystal stabilization in all the compounds comes from the Coulombic component (40.5–47.8%) only for molecular pairs involving N–H···S interactions, while for the remaining interactions, the dispersion energy is dominant.

The four chloro-substituted compounds here analyzed (**1**, **2**, IJUGEA, and DUNZIW) presented the higher lattice energy values, indicating the relevant role of the chlorine atom in the crystal stabilization of these compounds. In these molecules, weak C–H···Cl hydrogen bonds are formed, creating dimers where the cohesive energy ranges from −10 kJ mol^{-1} for DUNZIW to −25.4 kJ mol^{-1} for structure **2**. On the other hand, the VAGSUR and IMARIY compounds present similar dispersion (−127.3 and −133.1 kJ mol^{-1}) and total lattice energies (−131.8 and −133.1 kJ mol^{-1}). In the case of the FAXVOQ-I and FAXVOQ-II polymorphic forms, the cohesive energy in the lattice is very similar, with the former being more stable only by 1.5 kJ mol^{-1}. This suggests that changes in the space symmetry do not alter the total lattice energy of the unsubstituted compound.

The crystal packing of structure **1** is also characterized by the appearance of C–H···S hydrogen bonds generating $R_2^2(12)$ motifs (−48.7 kJ mol^{-1}), which alternate with strong $R_2^2(8)$ ring patterns along the *a* axis (Fig. S2†). In the case of structure **2**,

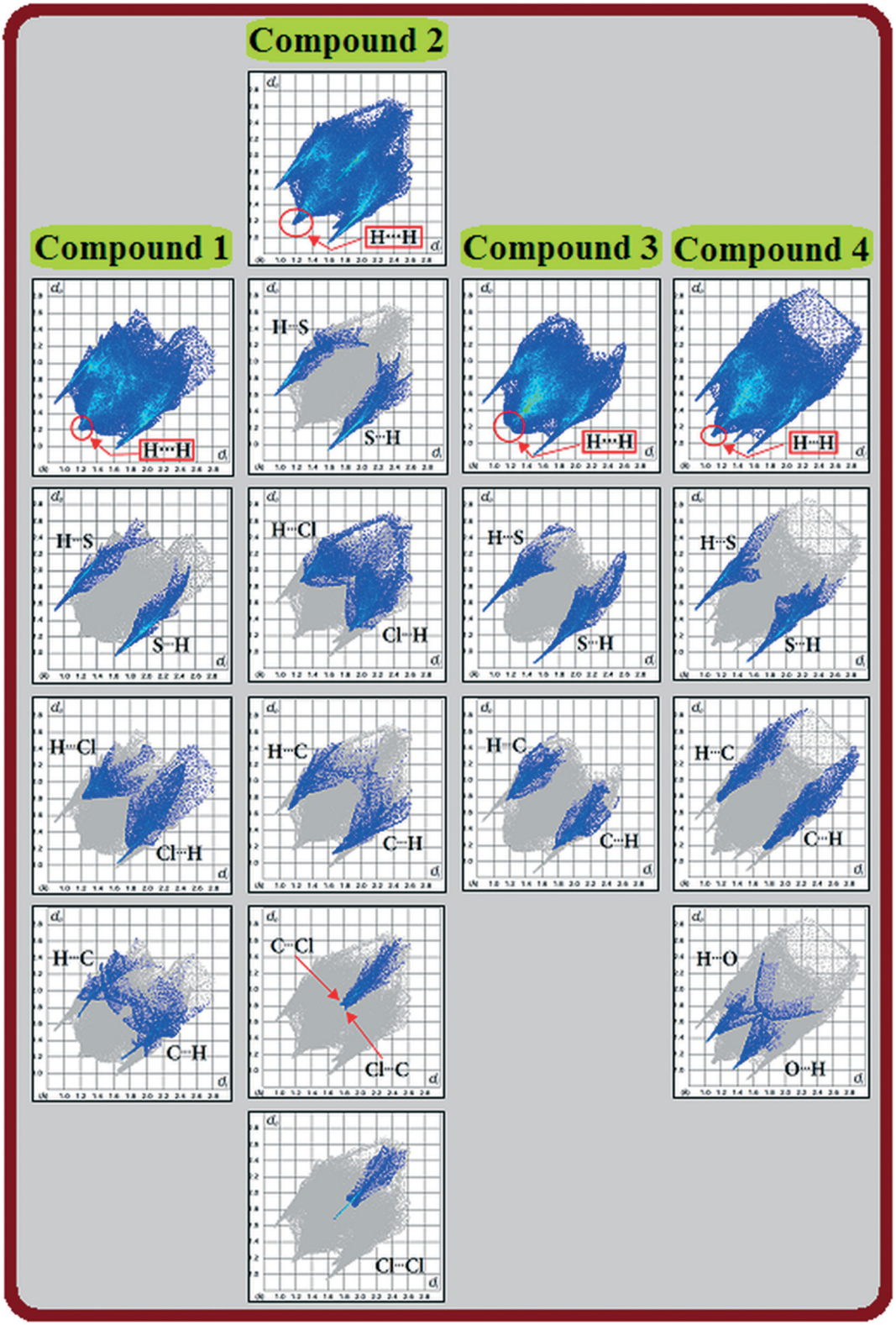

Fig. 7 Full and decomposed 2D fingerprint plots of the intermolecular contacts for **1–4**.

the lower Coulombic contribution of 40.5% can be attributed to an alternating combination of N–H···S and C–H···S hydrogen bonds forming weaker $R_2^2(10)$ dimers (Fig. S3†) in the two different molecular pairs with the same pairing energy (−61.0 kJ mol^{-1}). Unlike in the remaining structures, the $R_2^2(8)$ rings involved in a molecular pair amount to up to 78.7

kJ mol^{-1} and are interconnected by weaker C–H···S hydrogen bonds in structure **3** (Fig. S4, ESI†), which are associated with a lower intermolecular energy (−28.2 kJ mol^{-1}).

In structure **4**, a $R_2^2(14)$ descriptor was also observed interacting through weak C–H···S hydrogen bonds, as well as weak C–H···O hydrogen bonds due to the C7 atom in the molecule at (x, y, z) acting as a donor to the O1 atom of the methoxy group in the molecule at ($2 - x$, $-y$, $1 - z$). This interaction generates dimers (−11.2 kJ mol^{-1}) together with the formation of $R_2^2(6)$ rings (Fig. S5, ESI†) and a long intercentroid distance of 12.869 Å. Another molecular pair involves C–H···O hydrogen bonds with an increased intermolecular energy (−27.8 kJ mol^{-1}) and a shorter centroid distance of 8.729 Å.

The Hirshfeld surface analysis results were in sound agreement with the computed interaction energy values. Thus, the large and red regions labeled 1 in Fig. 6 are dominant in the d_{norm} maps for all the compounds, and represent H···S contacts attributed to N–H···S hydrogen bonds, which form $R_2^2(8)$ cyclic dimers through the two larger and very close regions exhibiting a similar brightness, as in structures **1**, **3**, and **4**. In the case of structure **2**, the two larger red spots are apart from each other and exhibit different brightnesses, indicating the combined participation of N–H and C–H donors and where the sulfur atom acts as a bifurcated acceptor. In compounds **1** and **2**, a pale blue to white spot labeled 2 on the front view of the surfaces shows Cl···H contacts associated with weak C–H···Cl hydrogen bonds. In compound **1**, distinctively to the others, a small red region labeled 6 depicts the presence of C···C contacts, indicating π-stacking interactions [characterized by Cg···Cg = 4.104(1) Å and slippage = 2.435(1) Å], providing additional stabilization (−43.0 kJ mol^{-1}) to the crystal packing (see also Fig. S6†).

In all the structures, the significant presence of H···H, S···H, and C···H contacts were found. The H···H interactions are highlighted in the middle of scattered points in the full 2D fingerprint maps, with minimum values of (d_e + d_i) around 2.4 Å. As expected, the H···H contacts are associated with molecular pairs with intermolecular energies (Table S7, ESI†) lower than −15 kJ mol^{-1} for most of structures, as the dispersive forces are the highest contributor (56–93%) toward the packing stabilization, with E_{disp} values from −7.4 to −45.7 kJ mol^{-1}. The repulsion energy values are in the range 3.1–27.3 kJ mol^{-1}.

Cl···H/H···Cl interactions are present in the two chloro-substituted compounds (**1**–**2**). In structure **1**, two asymmetrical spikes appear in the fingerprint plot, which spread up to the shorter distance of (d_e + d_i) ≈ 2.67 Å in the bottom-right region, and (d_e + d_i) ≈ 3.03 Å in the top-left region, which indicate Cl···H/H···Cl contacts occurring between molecules A and B in the asymmetric unit. The fingerprint plot of **2** (d_e + d_i ≈ 3.10 Å) displays two symmetrical sharp spikes, contributing 22.5% to the Hirshfeld surface area. The contributions to the Hirshfeld surface area due to Cl···H/H···Cl contacts are similar for monochloro-substituted compounds **1** (14.6%) and IJUGEA (15.8%, which is in good agreement with the value of 16.3% reported in ref. 51), while significant Cl···C/C···Cl and Cl···Cl contacts were found for compound **2**, comprising 5.1% and 3.7%, respectively.

The molecular ESP for molecule A of structure **1** (Fig. S9a, ESI†) revealed a highly polar molecule with a deep red region of strongly negative electrostatic potential (−0.082 au) surrounding the S2 atom, and a complementary deep blue region of strongly positive electrostatic potential (0.112 au) near the H1A hydrogen atom. These ESP values favor the formation of strong N–H···S contacts in this structure, supported by the high intermolecular energy value of −68.2 kJ mol^{-1}. In addition, an electronegative C–Cl group (−0.017 au on the surface) and an electropositive C–H group (0.043 au) are responsible for the formation of H···Cl contacts, which are electrostatically favored, and represent the weakest C207–H20G···Cl1 hydrogen bond interaction (−15.9 kJ mol^{-1}) in the self-assembly of structure **1**.

For the 2,3-di-chloro-substituted compound **2**, a high electropositive potential can be observed near the H atoms involving N–H···S (0.174 au) and C–H···S (0.139 au) hydrogen bonds (Fig. S10a, ESI†). These two intermolecular contacts are associated with a molecular pair with the highest interaction energy (−61.0 kJ mol^{-1}). It is interesting to note the reduced electronegative potentials of −0.027 and −0.022 au around the S1 atom in structure **2**. This can be explained considering that the sulfur atom participates as an acceptor in the formation of four hydrogen bonds, while the total negative charge is distributed around the periphery of the S1 atom.

The molecular ESP surface for structure **3** (Fig. S11a, ESI†) displays similar electrostatic features to that in structure **1**, with a deep red region of strongly electronegative potential (−0.086 au) surrounding the S1 atom, and a complementary deep blue area of strongly electropositive potential (0.117 au) near the H1A hydrogen atom.

Like in structures **1**–**3**, the ESP map of structure **4** (Fig. S12a†) shows strong N2–H2···S1 hydrogen bonds (−78.0 kJ mol^{-1}) as a result of the high electrostatic interaction (−0.087/0.109 au) between complementary regions. Moreover, an electronegative O-atom and an electropositive H7B hydrogen atom with lower potentials of −0.063 and 0.018 au, respectively, give rise to weaker C–H···O hydrogen bonds, forming $R_2^2(6)$ motifs associated with a molecular pair with minor interaction energy (−11.2 kJ mol^{-1}).

3D deformation density maps through the common N–H···S hydrogen bonds for compounds **1**–**4** (Fig. S9b–12b, ESI†) and additionally the Cl···Cl halogen bond[56] for structure **2** (Fig. S10b†) were also calculated for a better comprehension of the attractive nature of these interactions. It was clearly visible in all structures that the charge concentrated (CC) region around the S-atom is attracted toward the charge depleted (CD) region on the H-atom of the NH group in a neighboring molecule, confirming the formation of $R_2^2(8)$ cyclic dimers through N–H···S hydrogen bonds. Finally, the map of structure **2** (Fig. S10b†) displays an interaction between two CD regions representing a Cl2···Cl2

halogen bond, associated with a slightly attractive interaction (the E_{TOT} is −4.1 kJ mol^{-1}, see Table 3). The characteristic asphericity of the electron distribution around terminally-bonded chlorine atoms[57] reflects the high repulsion component of the lattice energy (9.1 kJ mol^{-1}, see Table 3) for this molecular pair.

5 Conclusions

The crystal structures of four 4,4,6-trimethyl-3,4-dihydropyrimidine-2(1*H*)-thione derivatives were determined by single-crystal X-ray diffraction. A complete investigation of the crystal packing was performed, including a comparison with eight closely related structures. Lattice energy determination indicated that the Coulombic component had a relevant contribution (of around 30%) to the total energy for all the compounds. In the same direction, the intermolecular interaction energies of selected molecular dimers indicated the maximum contribution (40.5–47.8%) toward the lattice stabilization came from the Coulombic component. Topological analysis and Hirshfeld surfaces studies gave a visual 3D picture of the nature of the intermolecular interactions in structures **1–4**, highlighting the strongest C═S···H contacts. The ESP and deformation density maps allowed a visual study of the electrostatic nature of the intermolecular N–H···S═C hydrogen bonds in the crystal stabilization.

The presence of halogen substituents, mainly Cl atoms, offers the possibility of establishing further intermolecular interactions. The electrostatic potentials calculated for the three types of hydrogen bonds observed in the crystal packing varied in the same way for both chloro-substituted compounds, being highest for the N–H···S hydrogen bond and lowest for the C–H···Cl hydrogen bond. This is a clear evidence of the relative strength of these interactions, decreasing in the order N–H···S > C–H···S > C–H···Cl for compounds **1–4**.

In summary, the nature of the intermolecular interactions in the crystal structures of the dihydropyrimidine derivatives was fully analyzed, and it could be useful for the prediction of supramolecular motifs in this type of compounds. The occurrence of N–H···S═C hydrogen bonds forming $R_2^2(8)$ motifs can be anticipated for the 3,4-dihydropyrimidine-2(1*H*)-thione group. This interaction is governed by the Coulombic components, with a minor influence of the 1-phenyl substitution.

Acknowledgements

ACF and MFE are members of the Carrera del Investigador of CONICET (República Argentina). The Argentine authors thank the Consejo Nacional de Investigaciones Científicas y Técnicas (CONICET), the ANPCYT (PICT-2130), and the Facultad de Ciencias Exactas, Universidad Nacional de La Plata for financial support. HP and MFE also thank the Programa Redes (Ministerio de Educación, Argentina).

References

1 J. D. Dunitz and A. Gavezzotti, *Cryst. Growth Des.*, 2012, **12**, 5873–5877.
2 G. R. Desiraju, *Angew. Chem., Int. Ed.*, 2011, **50**, 52–59.
3 F. F. Ferreira, A. C. Trindade, S. G. Antonio and C. de Oliveira Paiva-Santos, *CrystEngComm*, 2011, **13**, 5474–5479.
4 K. S. Eccles, R. E. Morrison, A. R. Maguire and S. E. Lawrence, *Cryst. Growth Des.*, 2014, **14**, 2753–2762.
5 K. S. Eccles, R. E. Morrison, A. S. Sinha, A. R. Maguire and S. E. Lawrence, *Cryst. Growth Des.*, 2015, **15**, 3442–3451.
6 D. Dey, T. P. Mohan, B. Vishalakshi and D. Chopra, *Cryst. Growth Des.*, 2014, **14**, 5881–5896.
7 I. Wawrzycka-Gorczyca, *J. Struct. Chem.*, 2014, **55**, 520–524.
8 S. B. Novaković, B. Fraisse, G. A. Bogdanović and A. Spasojević-de Biré, *Cryst. Growth Des.*, 2007, **7**, 191–195.
9 A. Saeed and M. Bolte, *Acta Crystallogr., Sect. E: Struct. Rep. Online*, 2010, **66**, o440.
10 A. Saeed, R. A. Khera and M. Parvez, *Acta Crystallogr., Sect. E: Struct. Rep. Online*, 2010, **66**, o635.
11 P. Biginelli, *Ber. Dtsch. Chem. Ges.*, 1891, **24**, 1317–1319.
12 P. Biginelli, *Ber. Dtsch. Chem. Ges.*, 1891, **24**, 2962–2967.
13 Á. de Fátima, T. C. Braga, L. D. S. Neto, B. S. Terra, B. G. F. Oliveira, D. L. da Silva and L. V. Modolo, *J. Adv. Res.*, 2015, **6**, 363–373.
14 S. Andleeb, D. Imtiaz ud, M. K. Rauf, S. S. Azam, A. Badshah, H. Sadaf, A. Raheel, M. N. Tahir and S. Raza, *RSC Adv.*, 2016, **6**, 79651–79661.
15 R. F. W. Bader, J. R. Cheeseman, K. E. Laidig, K. B. Wiberg and C. Brenemad, *J. Am. Chem. Soc.*, 1990, **112**, 6530–6536.
16 J. D. Dunitz and A. Gavezzotti, *Chem. Soc. Rev.*, 2009, **38**, 2622–2633.
17 A. Gavezzotti, *New J. Chem.*, 2011, **35**, 1360–1368.
18 S. K. Seth, I. Saha, C. Estarellas, A. Frontera, T. Kar and S. Mukhopadhyay, *Cryst. Growth Des.*, 2011, **11**, 3250–3265.
19 S. K. Seth, D. Sarkar, A. D. Jana and T. Kar, *Cryst. Growth Des.*, 2011, **11**, 4837–4849.
20 A. Saeed, M. Bolte, M. F. Erben and H. Perez, *CrystEngComm*, 2015, **17**, 7551–7563.
21 M. Owczarek, I. Majerz and R. Jakubas, *CrystEngComm*, 2014, **16**, 7638–7648.
22 P. Panini and D. Chopra, *Cryst. Growth Des.*, 2014, **14**, 3155–3168.
23 B. M. Yamin, N. A. M. Kasim and N. Hamzah, *Acta Crystallogr., Sect. E: Struct. Rep. Online*, 2005, **61**, o55–o57.
24 N. L. Ismail, E. Othman and B. M. Yamin, *Acta Crystallogr., Sect. E: Struct. Rep. Online*, 2007, **63**, o2442–o2443.
25 A. Saeed, R. A. Khera and U. Flörke, *Structural Chemistry Communications*, 2010, **1**, 63–64.
26 G. Sheldrick, *Acta Crystallogr., Sect. A: Found. Crystallogr.*, 2008, **64**, 112–122.
27 A. Spek, *Acta Crystallogr., Sect. D: Biol. Crystallogr.*, 2009, **65**, 148–155.
28 O. V. Dolomanov, L. J. Bourhis, R. J. Gildea, J. A. K. Howard and H. Puschmann, *J. Appl. Crystallogr.*, 2009, **42**, 339–341.

29 C. F. Macrae, I. J. Bruno, J. A. Chisholm, P. R. Edgington, P. McCabe, E. Pidcock, L. Rodriguez-Monge, R. Taylor, J. van de Streek and P. A. Wood, *J. Appl. Crystallogr.*, 2008, **41**, 466–470.

30 R. Dovesi, V. R. Saunders, C. Roetti, R. Orlando, C. M. Zicovich-Wilson, F. Pascale, B. Civalleri, K. Doll, N. M. Harrison, I. J. Bush, P. D'Arco, M. Llunell, M. Causà and Y. Noël, *CRYSTAL14 User's Manual*, University of Torino, Torino, 2014.

31 C. Gatti, V. R. Saunders and C. Roetti, *J. Chem. Phys.*, 1994, **101**, 10686–10696.

32 C. Gatti and S. Casassa, *TOPOND User's Manual*, CNR-ISTM of Milano, Milano, 2014.

33 A. Gavezzotti, *J. Phys. Chem. B*, 2003, **107**, 2344–2353.

34 A. Gavezzotti, *J. Phys. Chem. B*, 2002, **106**, 4145–4154.

35 J. J. McKinnon, M. A. Spackman and A. S. Mitchell, *Acta Crystallogr., Sect. B: Struct. Sci.*, 2004, **60**, 627–668.

36 J. J. McKinnon, D. Jayatilaka and M. A. Spackman, *Chem. Commun.*, 2007, 3814–3816.

37 M. A. Spackman and D. Jayatilaka, *CrystEngComm*, 2009, **11**, 19–32.

38 M. A. Spackman, *Chem. Rev.*, 1992, **92**, 1769–1797.

39 S. K. Wolff, D. J. Grimwood, J. J. McKinnon, M. J. Turner, D. Jayatilaka and M. A. Spackman, *CrystalExplorer (Version 3.1)*, University of Western Australia, 2012.

40 M. A. Spackman, *Phys. Scr.*, 2013, **87**, 048103.

41 D. Jayatilaka, D. J. Grimwood, A. Lee, A. Lemay, A. J. Russel, C. Taylor, S. K. Wolff, P. Cassam-Chenai and A. Whitton, *TONTO – A System for Computational Chemistry*, 2005.

42 T. Gelbrich and M. B. Hursthouse, *CrystEngComm*, 2005, **7**, 324–336.

43 N. Anuradha, A. Thiruvalluvar, K. Pandiarajan, S. Chitra and R. J. Butcher, *Acta Crystallogr., Sect. E: Struct. Rep. Online*, 2009, **65**, o564–o565.

44 N. Anuradha, A. Thiruvalluvar, K. Pandiarajan, S. Chitra and R. J. Butcher, *Acta Crystallogr., Sect. E: Struct. Rep. Online*, 2009, **65**, o3068.

45 D. Cremer and J. A. Pople, *J. Am. Chem. Soc.*, 1975, **97**, 1354–1358.

46 E. Espinosa, M. Souhassou, H. Lachekar and C. Lecomte, *Acta Crystallogr., Sect. B: Struct. Sci.*, 1999, **55**, 563–572.

47 I. Dance, *New J. Chem.*, 2003, **27**, 1–2.

48 F. Allen, *Acta Crystallogr., Sect. B: Struct. Sci.*, 2002, **58**, 380–388.

49 I. J. Bruno, J. C. Cole, P. R. Edgington, M. Kessler, C. F. Macrae, P. McCabe, J. Pearson and R. Taylor, *Acta Crystallogr., Sect. B: Struct. Sci.*, 2002, **58**, 389–397.

50 B. M. Yamin and H. F. Salem, *Acta Crystallogr., Sect. E: Struct. Rep. Online*, 2011, **67**, o282.

51 M. G. Babashkina, K. Robeyns, Y. Filinchuk and D. A. Safin, *New J. Chem.*, 2016, **40**, 1230–1236.

52 B. M. Yamin, R. L. Lawi and H. F. Salem, *Acta Crystallogr., Sect. E: Struct. Rep. Online*, 2011, **67**, o1810.

53 R. Fröhlich and G. D. Nigam, *Z. Kristallogr.*, 1987, **180**, 151–155.

54 M. A. Spackman, J. J. McKinnon and D. Jayatilaka, *CrystEngComm*, 2008, **10**, 377–388.

55 T. Gelbrich, T. L. Threlfall and M. B. Hursthouse, *CrystEngComm*, 2012, **14**, 5454–5464.

56 P. Metrangolo, H. Neukirch, T. Pilati and G. Resnati, *Acc. Chem. Res.*, 2005, **38**, 386–395.

57 S. L. Price, A. J. Stone, J. Lucas, R. S. Rowland and A. E. Thornley, *J. Am. Chem. Soc.*, 1994, **116**, 4910–4918.

